SUPPORTING INFORMATION

Inducing differential self-assembling behaviour in ultrashort peptide hydrogelators using simple metal salts

Pooja Sharma[a], Harsimran Kaur[a], and Sangita Roy[a]*

[a]Institute of Nanoscience and Technology, Habitat centre, sector 64, phase 10, Mohali, Punjab, 160062

Table of contents:

^{1}H and ^{13}C NMR characterization of histidine based dipeptide amphiphiles.

1. **Table S1.** LC-MS data.
2. **Table S2.** cLogP values, minimum gelation concentration (MGC) and optical images of hydrogels formed by histidine based peptide amphiphiles.
3. **Table S3.** Minimum gelation concentration of Fmoc-HL-COOH in the presence of metal salts.
4. **Figure S1.** Reverse-phase HPLC chromatogram and Mass spectra of synthesized histidine based dipeptides.
5. **Figure S2.** RP-HPLC and LC-MS analysis confirming the integrity of fmoc group during gelation.
6. **Figure S3.** ^{1}H-NMR spectrum of Fmoc-HL-COOH lyophilized hydrogel, demonstrating the integrity of the fmoc group during gelation.
7. **Figure S4.** ^{13}C-NMR spectrum of of Fmoc-HL-COOH hydrogel showing the integrity of the fmoc group during gelation.
8. **Figure S5.** Variation in fluorescence intensity of ThT during transition from sol to gel state for peptide amphiphile Fmoc-HL-COOH and Fmoc-HS-COOH.
9. **Figure S6.** Fluorescence microscopic images of dipeptide hydrogels after incubation with thioflavin-T.
10. **Figure S7.** AFM images of Fmoc-HL-COOH at different time intervals after gelation showing the growth of the fibers.
11. **Figure S8.** Strain sweep analysis of histidine based hydrogels, (a) Fmoc-HF-COOH, (b) Fmoc-HL-COOH, (c) Fmoc-HV-COOH, (d) Fmoc-HS-COOH.
12. **Figure S9.** Mechanical strength characterization of Fmoc-HL-COOH hydrogel at variable pH as measured using oscillatory rheology.
13. **Figure S10.** Representative RP-HPLC and LC-MS analysis confirming the integrity of fmoc group during gelation in the presence of metal salts.
14. **Figure S11.** ^{1}H-NMR spectrum of lyophilized hydrogel of Fmoc-HL-COOH formed in the presence of iron (II) chloride, showing significant NMR peak broadening.
15. **Figure S12.** ^{1}H-NMR spectrum of lyophilized hydrogel of Fmoc-HL-COOH formed in the presence of copper (II) chloride, showing significant NMR peak broadening.

16. **Figure S13.** ^{1}H-NMR spectrum of lyophilized hydrogel of Fmoc-HL-COOH formed in the presence of magnesium chloride, demonstrating the integrity of the fmoc group during gelation.
17. **Figure S14.** ^{13}C-NMR spectrum of lyophilized hydrogel of Fmoc-HL-COOH formed in the presence of magnesium chloride, demonstrating the integrity of the fmoc group during gelation.
18. **Figure S15.** UV-Vis spectra of Fmoc-HL-COOH in the presence of various metal salts suggesting the complex formation.
19. **Figure S16.** Strain sweep analysis of (a) Fmoc-HL-COOH at 10 mM, Fmoc-HL-COOH (10 mM) in the presence of (b) iron (II) chloride (10 mM), (c) copper (II) chloride (10 mM), (d) magnesium chloride (10 mM).
20. **Figure S17.** Mechanical strength of Fmoc-HL-COOH (10 mM) in the presence of salts at a concentration of 10 mM each.
21. **Figure S18.** Strain sweep analysis of Fmoc-HL-COOH (20 mM) in the presence of (a) iron (II) chloride, (b) manganese chloride, (c) nickel chloride, (d) copper (II) chloride.
22. **Figure S19.** Strain sweep analysis of Fmoc-HL-COOH in the presence of (a) iron (II) chloride (1:1), (b) iron (II) chloride (1:2), (c) copper (II) chloride (1:1), (d) copper (II) chloride (1:2).
23. **Figure S20.** Variation in mechanical strength of Fmoc-HL-COOH with varying ratio of iron (II) chloride and copper (II) chloride as measured by oscillatory rheology
24. **Figure S21.** Magnified view of figure 7e showing the fluorescence spectra of Fmoc-HL-COOH in the presence of iron (II) chloride and manganese chloride depicting the quenching of fmoc fluorescence upon gelation.
25. **Figure S22**. Strain sweep analysis of Fmoc-HL-COOH hydrogel formed in the presence of (a) magnesium citrate, (b) magnesium chloride, (c) magnesium iodide.
26. **Figure S23.** Strain sweep analysis of Fmoc-HL-COOH hydrogel formed in the presence of (a) magnesium chloride (1:1), (b) magnesium chloride (1:2).
27. **Figure S24.** Variation in mechanical strength of Fmoc-HL-COOH with varying ratio of magnesium chloride as measured by oscillatory rheology.
28. **Figure S25.** Spectroscopic characterization of hydrogels formed by Fmoc-HL-COOH in the presence of magnesium salts.

29. **Figure S26.** Spectra representing the variation in HT with wavelength for dipeptide hydrogels and hydrogels formed in the presence various salts.

Analytical characterization of histidine based dipeptide amphiphiles using ^{1}H and ^{13}C NMR.

Fmoc-HF-COOH:

^{1}H NMR (400 MHz, DMSO-d_6):δ 14.2-13.8 (broad peak, 1H), δ 8.94-8.93 (d, 1H), δ 8.12-8.10 (d, 2H), δ 7.86-7.84 (d, 2H), δ 7.67 (s,1H), δ 7.65-7.63 (d, 2H), δ 7.43-7.38 (t, 2H), δ 7.33-7.32 (m, 2H), δ 7.30-7.29 (m, 2H), δ 7.28-7.26 (m,2H), 7.23-7.20 (m, 1H), δ 4.52-4.49 (m, 1H), δ 4.42-4.40 (m, 1H), δ 4.28-4.27 (d, 2H), δ 4.26-4.25 (m,1H), δ 3.13-3.10 (m, 1H), δ 3.09-3.06 (m, 1H), δ 2.99-2.95 (m,1H), δ 2.92-2.90 (m, 1H).

^{13}C NMR (100 MHz, DMSO-d_6):δ_c (ppm) =172.60 (phenylalanine, C=O), 170.26 (histidine, C=O), 155.74 (fmoc, C=O), 143.73 (fluorenyl aromatic –C), 140.67 (fluorenyl aromatic –C), 137.24 (phenylalanine, aromatic –C), 133.78 (imidazole, aromatic –C), 129.52 (imidazole, aromatic –C), 128.14 (phenylalanine, -CH), 127.74 (phenylalanine, aromatic -CH), 127.49 (fluorenyl, aromatic -CH) 127.05 (fluorenyl, aromatic –CH), 126.44 (phenylalanine, aromatic –CH), 125.21 (phenylalanine, aromatic –CH), 125.2 (fluorenyl, aromatic –CH), 120.10 (fluorenyl, aromatic –CH), 116.77 (imidazole, aromatic –CH), 65.77 (fluorenyl aliphatic –CH_2), 53.51 (phenylalanine, α-CH), 53.43 (histidine, α-CH), 46.50 (fluorenyl, -CH), 36.46 (phenylalanine, side chain –CH_2), 26.91 (histidine, side chain –CH_2).

Fmoc-HL-COOH:

^{1}H NMR (400 MHz, DMSO-d_6):δ 14.36 (broad peak, 1H), δ 8.84 (d, 1H), δ 8.10-8.07 (d, 2H), δ 7.81-7.79 (d, 2H), δ 7.66-7.62 (m, 1H), δ 7.57-7.55 (d, 2H), δ 7.42-7.38 (t, 2H), δ 7.33-7.27 (m, 2H), δ 4.51-4.45 (m, 1H), δ 4.35-4.33 (m, 2H), δ 4.31-4.28 (m, 1H), δ 4.27-4.16 (m, 1H), δ 3.22-3.17 (m, 1H), δ 3.05-2.99 (m, 1H), δ 1.71-1.66 (m, 2H), δ 1.60-1.57 (m, 1H), δ 0.92-0.84 (m, 6H).

^{13}C NMR (100 MHz, DMSO-d$_6$): δ_c (ppm) = 173.86 (leucine, C=O), 170.34 (histidine,C=O), 155.76 (fmoc, C=O), 143.73 (fluorenyl, aromatic –C), 140.66 (fluorenyl aromatic –C), 133.76 (imidazole aromatic –CH), 129.58 (imidazole aromatic –C), 127.62 (fluorenyl, -CH), 127.04 (fluorenyl, -CH), 125.21 (fluorenyl, -CH), 120.09 (fluorenyl, -CH), 116.79 (imidazole, -CH), 65.74 (fluorenyl, aliphatic –CH_2), 53.38 (histidine, α-CH), 50.39 (leucine, α-CH), 46.52 (fluorenyl, -CH), 40.04 (leucine, side chain –CH_2), 27.01 (histidine, side chain –CH_2), 24.19 (leucine, side chain aliphatic –CH), 22.79 (leucine, side chain –CH_3).

Fmoc-HV-COOH:

^{1}H NMR (400 MHz, DMSO-d$_6$):δ 13.9 (broad peak, 1H), δ 8.85 (d, 1H), δ 7.86-7.84 (d, 2H), δ 7.81-7.79 (d, 2H), δ 7.66-7.61 (m, 1H), δ 7.41-7.39 (d, 2H), δ 7.38-7.31 (m, 2H), δ 7.29-7.27 (m, 2H), δ 4.56-4.53 (m, 1H), δ 4.29-4.24 (m, 2H), δ 4.26-4.24 (m, 1H), δ 4.20-4.16 (m, 1H), δ 3.21-3.17 (m, 1H), δ 3.16-3.03 (m, 1H), δ 2.17-2.12 (m, 1H), δ 0.93-0.92 (m, 6H).

^{13}C NMR (100 MHz, DMSO-d$_6$): δ_c (ppm) = 172.71 (valine, C=O), 170.56 (histidine, C=O), 155.79 (fmoc, C=O), 143.71 (fluorenyl, aromatic –C), 140.66 (fluorenyl, aromatic –C), 133.77 (imidazole, -CH), 129.58 (imidazole, aromatic –C), 127.62 (fluorenyl, -CH), 127.04 (fluorenyl, -CH), 125.18 (fluorenyl, -CH), 120.09 (fluorenyl, -CH), 116.78 (imidazole, -CH), 65.72 (fluorenyl, aliphatic –CH_2), 57.21 (valine, α-CH), 53.36 (histidine, α-CH), 46.51 (fluorenyl, -CH), 29.76 (histidine, side chain –CH_2), 27.01 (valine, side chain –CH), 18.99 (valine, side chain –CH_3).

Fmoc-HS-COOH:

^{1}H NMR (400 MHz, DMSO-d$_6$):δ 14.2-13.8 (broad peak, 1H), δ 8.94 (d, 1H), δ 8.11-8.09 (d, 2H), δ 7.85-7.83 (d, 2H), δ 7.70-7.68 (m, 1H), δ 7.67-7.64 (m, 2H), δ 7.42-7.39(t, 2H), δ 7.30-

7.27 (t, 2H), δ 4.54-4.49 (m, 1H), δ 4.36-4.32 (m, 2H), δ 4.29-4.27 (d, 1H), δ 4.26-4.20 (m,1H), δ 4.18-4.16 (m, 1H), δ 3.84-3.80 (m, 1H), δ 3.71-3.67 (m, 1H), δ 3.19-3.14 (m, 1H), δ 3.03-2.97 (m, 1H).

^{13}C NMR (100 MHz, DMSO-d$_6$): δ_c (ppm) = 171.74 (histidine, C=O), 170.38 (serine, C=O), 155.81 (fluorenyl, C=O), 133.74 (imidazole, -CH), 129.55 (imidazole, aromatic –C), 127.63 (fluorenyl, -CH), 127.06 (fluorenyl, -CH), 125.21 (fluorenyl, -CH), 120.09 (fluorenyl,-CH), 116.81 (imidazole, -CH), 65.77 (fluorenyl, aliphatic –CH_2), 61.13 (serine, side chain –CH_2), 61.06 (serine, α-CH), 54.68 (histidine, α-CH), 46.50 (fluorenyl, -CH), 27.17 (histidine, side chain –CH_2).

^{1}H NMR analysis of lyophilized hydrogels of Fmoc-HL-COOH in the presence of metal salts.

Fmoc-HL-COOH

^{1}H NMR (400 MHz, DMSO-d$_6$): δ 14.16 (broad peak, 1H), δ 8.21-8.19 (d, 1H), δ 7.89-7.87 (d, 2H), δ 7.68-7.66 (d, 2H), δ 7.55-7.53 (d, 1H), δ 7.43-7.39 (m, 2H), δ 7.34-7.32 (m, 2H), δ 7.31-7.30 (m, 2H), δ 4.33-4.30 (m, 1H), δ 4.29-4.26 (m, 2H), δ 4.24-4.21 (m, 1H), δ 4.19-4.18 (m, 1H), δ 2.98-2.94 (m, 1H), δ 2.89-2.83 (m, 1H), δ 1.63-1.59 (m, 2H), δ 1.56-1.47 (m, 1H), δ 0.88-0.81 (m, 6H).

Fmoc-HL-COOH + Magnesium chloride

^{1}H NMR (400 MHz, DMSO-d$_6$): δ 14.16 (broad peak, 1H), δ 8.22-8.20 (d, 1H), δ 7.89-7.87 (d, 2H), δ 7.68-7.66 (d, 2H), δ 7.57-7.55 (d, 1H), δ 7.43-7.39 (m, 2H), δ 7.34-7.32 (m, 2H), δ 7.31-7.30 (m, 2H), δ 4.33-4.30 (m, 1H), δ 4.29-4.28 (m, 2H), δ 4.23-4.20 (m, 1H), δ 4.19-4.16 (m,

1H), δ 3.00-2.95 (m, 1H), δ 2.90-2.84 (m, 1H), δ 1.66-1.61 (m, 2H), δ 1.59-1.48 (m, 1H), δ 0.86-0.80 (m, 6H).

Fmoc-HL-COOH + Iron (II) chloride

^{1}H NMR (400 MHz, DMSO-d$_6$): Significant peak broadening occurred due to presence of transition metal salt.

Fmoc-HL-COOH + Copper (II) chloride

^{1}H NMR (400 MHz, DMSO-d$_6$): Significant peak broadening occurred due to presence of transition metal salt.

^{13}C NMR analysis of lyophilized hydrogels of Fmoc-HL-COOH in the presence of metal salts.

Fmoc-HL-COOH (Lyophilized hydrogel)

^{13}C NMR (100 MHz, DMSO-d$_6$): δ_c (ppm) = 174.33 (leucine, C=O), 171.19 (histidine,C=O), 155.63 (fmoc, C=O), 143.79 (fluorenyl, aromatic –C), 140.62 (fluorenyl aromatic –C), 134.58 (imidazole aromatic –CH), 129.54 (imidazole aromatic –C), 127.60 (fluorenyl, -CH), 127.07 (fluorenyl, -CH), 125.30 (fluorenyl, -CH), 120.06 (fluorenyl, -CH), 115.75 (imidazole, -CH), 65.67 (fluorenyl, aliphatic –CH_2), 54.37 (histidine, α-CH), 50.71 (leucine, α-CH), 46.54 (fluorenyl, -CH), 40.05 (leucine, side chain –CH_2), 29.31 (histidine, side chain –CH_2), 24.20 (leucine, side chain aliphatic –CH), 22.89 (leucine, side chain –CH_3).

Fmoc-HL-COOH + Magnesium chloride (Lyophilized hydrogel)

^{13}C NMR (100 MHz, DMSO-d$_6$): δ_c (ppm) = 174.98 (leucine, C=O), 170.05 (histidine,C=O), 155.67 (fmoc, C=O), 143.76 (fluorenyl, aromatic –C), 140.62 (fluorenyl aromatic –C), 134.27 (imidazole aromatic –CH), 128.21 (imidazole aromatic –C), 127.61 (fluorenyl, -CH), 127.07(fluorenyl, -CH), 125.28 (fluorenyl, -CH), 120.06 (fluorenyl, -CH), 118.67 (imidazole, -CH), 65.69 (fluorenyl, aliphatic –CH_2), 54.20 (histidine, α-CH), 50.67 (leucine, α-CH), 46.53 (fluorenyl, -CH), 40.02 (leucine, side chain –CH_2), 28.61 (histidine, side chain –CH_2), 24.20 (leucine, side chain aliphatic –CH), 21.29 (leucine, side chain –CH_3).

Table S1. m/z values different peptides from Chemdraw (Ultra 12.0) and ESI-MS.

Peptide amphiphile (Molecular formula)	**Calculated m/z value (M+1) (Chem Draw Ultra 12.0)**	**Found m/z value (M+1) (ESI-MS)**
Fmoc-HF-COOH ($C_{30}H_{28}N_4O_5$)	525.21	525.50
Fmoc-HL-COOH ($C_{27}H_{30}N_4O_5$)	491.22	491.43
Fmoc-HV-COOH ($C_{26}H_{28}N_4O_5$)	477.21	477.38
Fmoc-HS-COOH ($C_{24}H_{24}N_4O_6$)	465.17	465.43

Table S2. cLogP values, minimum gelation concentration (MGC) and optical images of hydrogels formed by histidine based peptide amphiphiles.

Peptide amphiphile	**Fmoc-HF-COOH**	**Fmoc-HL-COOH**	**Fmoc-HV-COOH**	**Fmoc-HS-COOH**
cLogP value	3.73	3.76	3.23	1.24
Minimum gelationconcentration (MGC) (mM)	20	10	15	15
Hydrogelsat physiological pH				

Table S3. Minimum gelation concentration of Fmoc-HL-COOH in the presence of metal salts.

Fmoc-HL-COOH Concentration (mM)	**Salt Concentration (mM)**					
	$MgCl_2$		**$FeCl_2$**		**$CuCl_2$**	
5	**10**	**Sol**	**10**	**Sol**	**10**	**Sol**
10	**10**	**Gel**	**10**	**Gel**	**10**	**Gel**
20	**10**	**Gel**	**10**	**Gel**	**10**	**Gel**

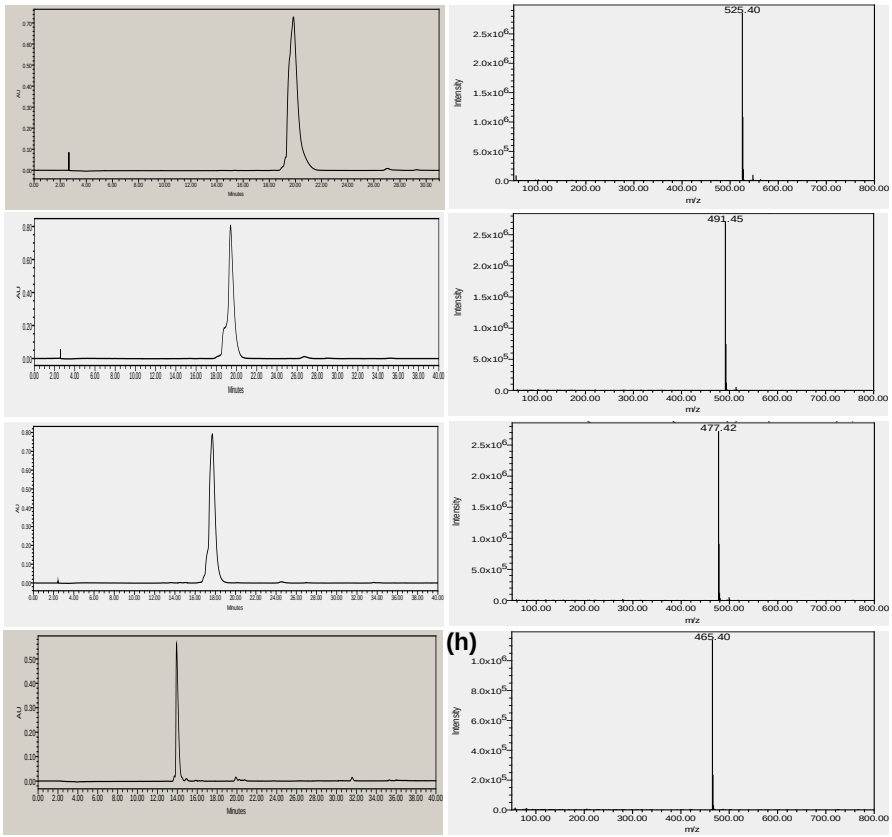

Figure S1. Reverse phase HPLC chromatogram and mass spectra of synthesized peptides respectively,(a, b) Fmoc-HF-COOH, (c, d) Fmoc-HL-COOH, (e, f) Fmoc-HV-COOH, (g, h) Fmoc-HS-COOH.

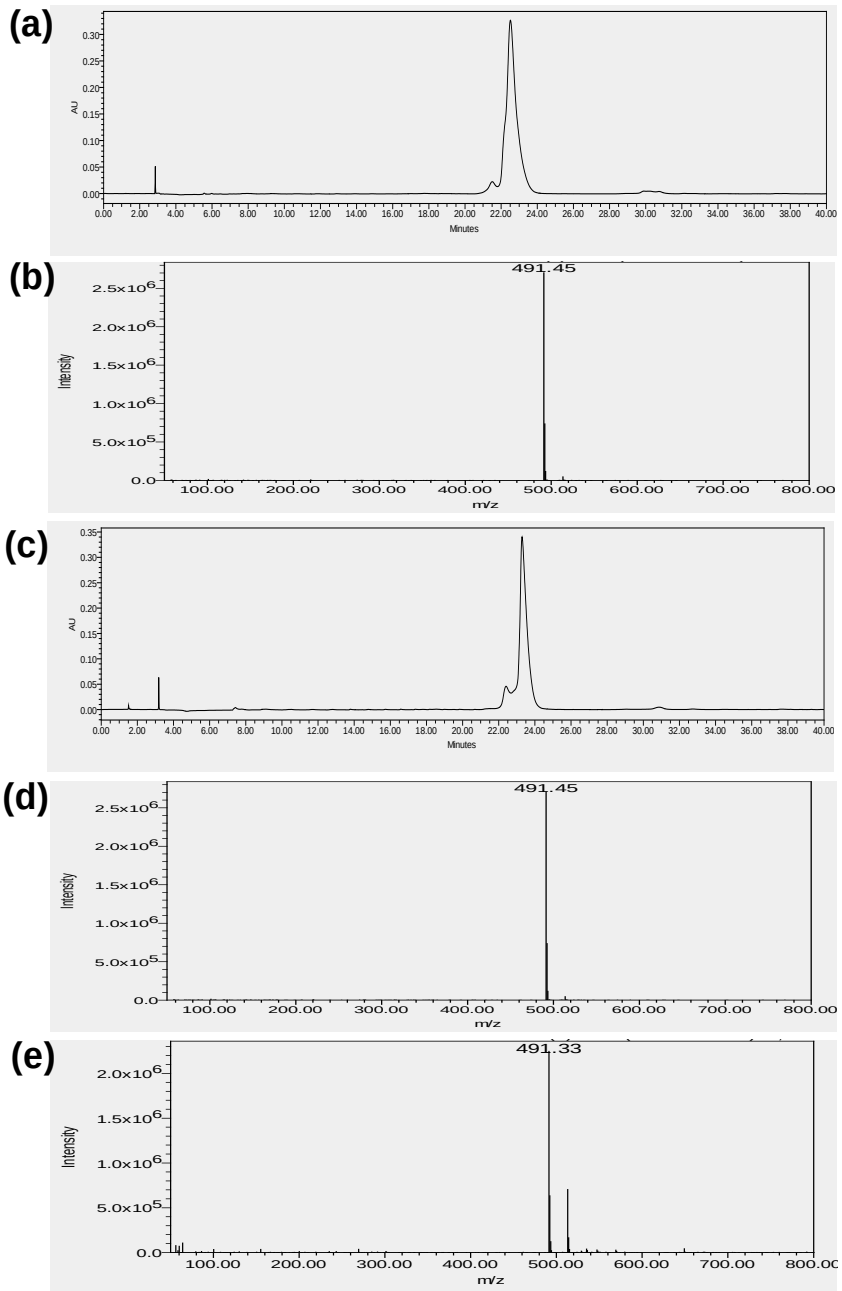

Figure S2. Representative HPLC chromatogram and mass spectra of Fmoc-HL-COOH, (a,b) immediately after adjusting the pH to 10.0, (c,d) and after pH was adjusted to 7.0 respectively, (e) Direct mass analysis of Fmoc-HL-COOH lyophilized hydrogel. Both the analysis confirmed that the pH adjusted for dissolution of peptides did not cleave the fluorenyl moiety from the peptide.

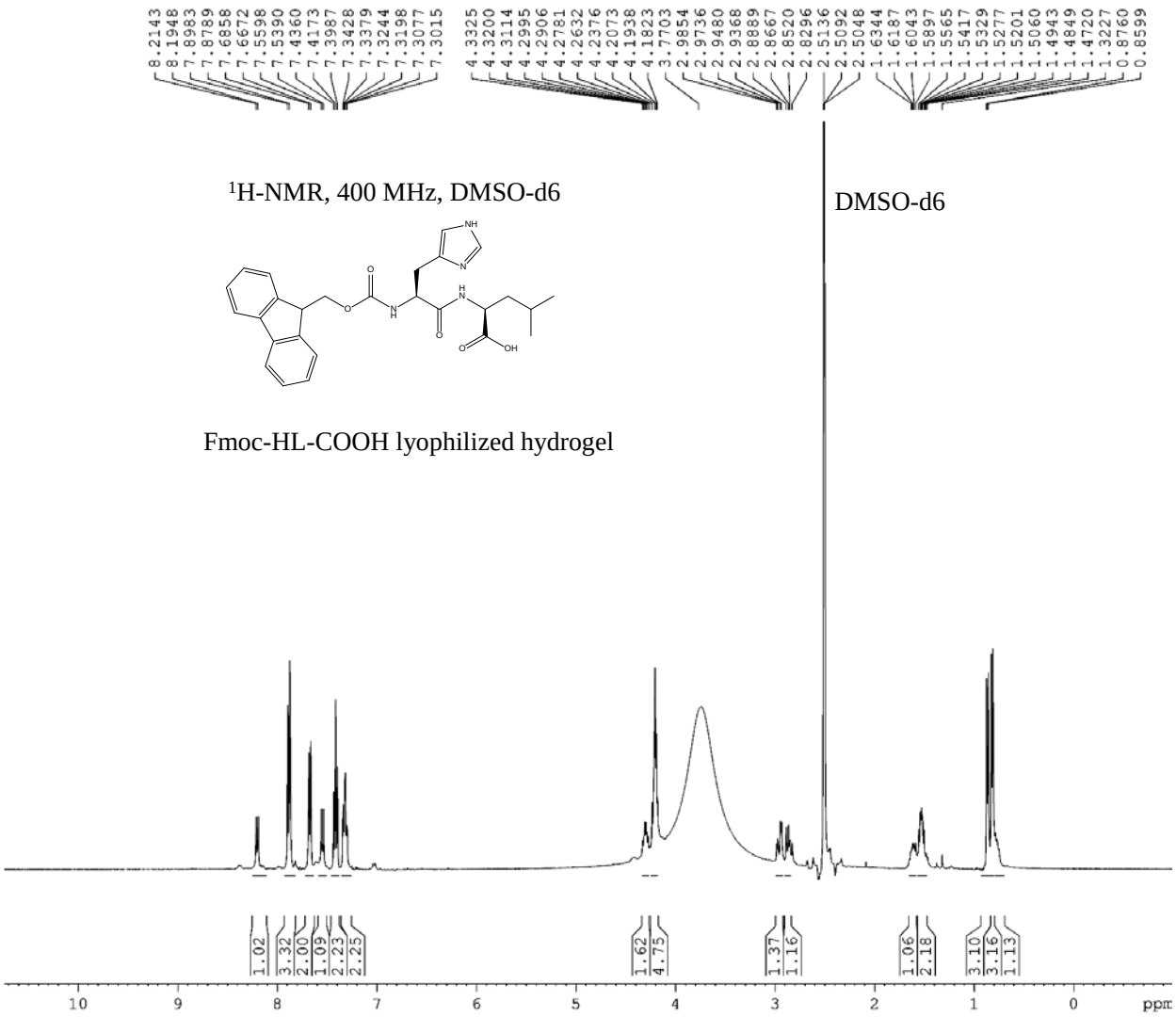

Figure S3. ^{1}H-NMR spectrum of Fmoc-HL-COOH lyophilized hydrogel, demonstrating the integrity of the fmoc group during gelation.

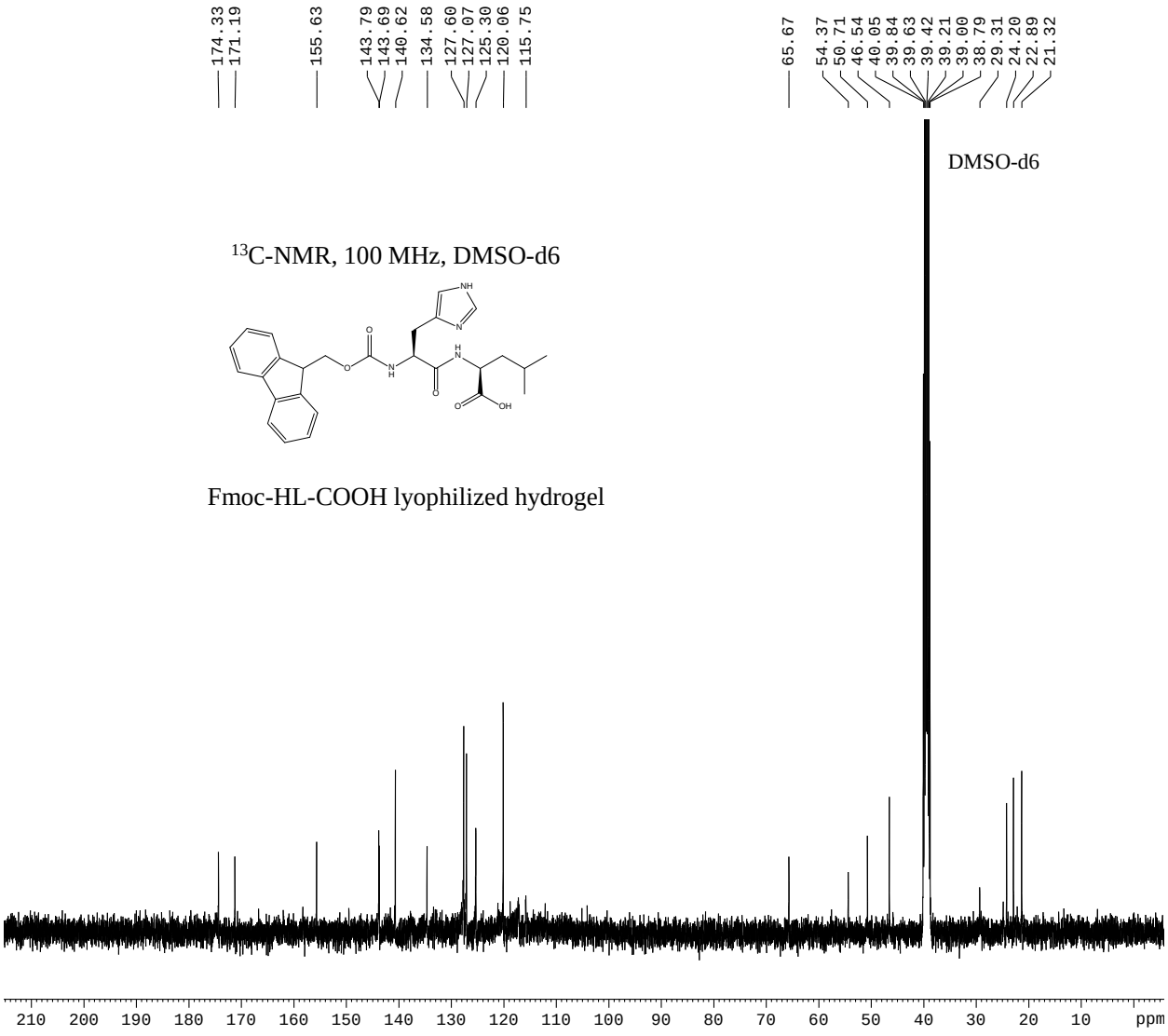

Figure S4. ^{13}C-NMR spectrum of of Fmoc-HL-COOH hydrogel showing the integrity of the fmoc group during gelation.

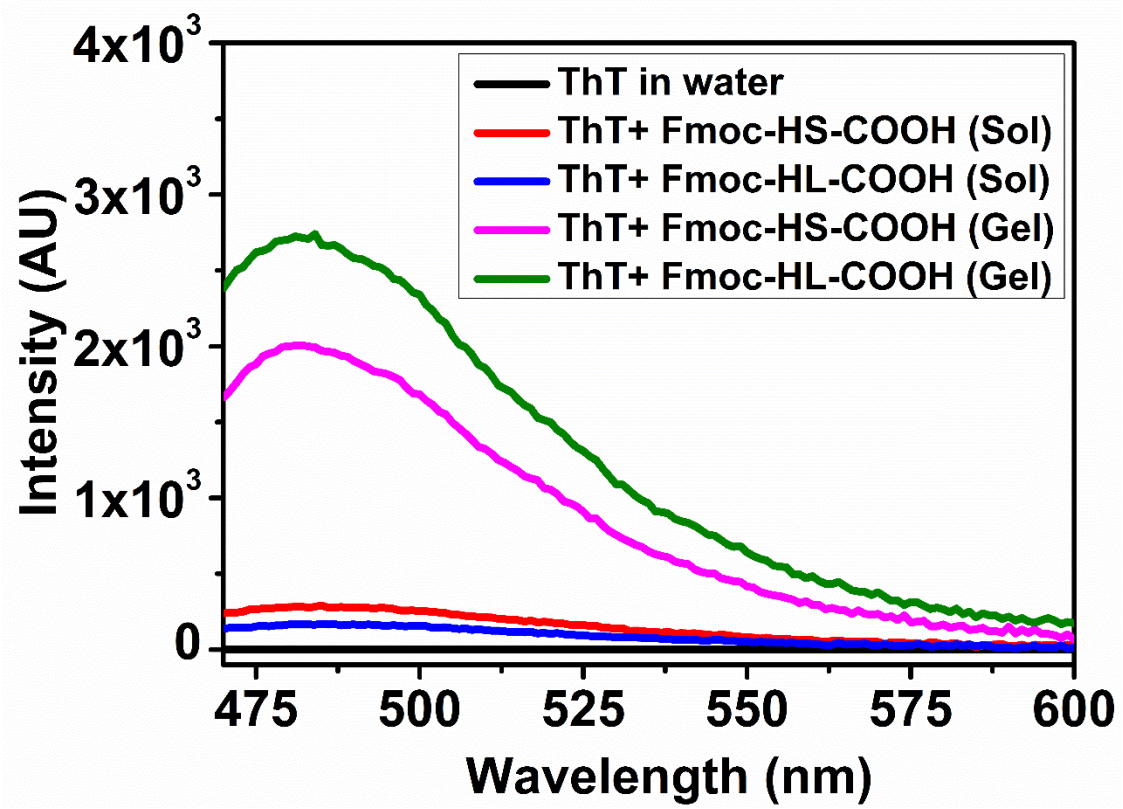

Figure S5. Variation in fluorescence intensity of ThT during transition from sol to gel state for Fmoc-HL-COOH and Fmoc-HS-COOH.

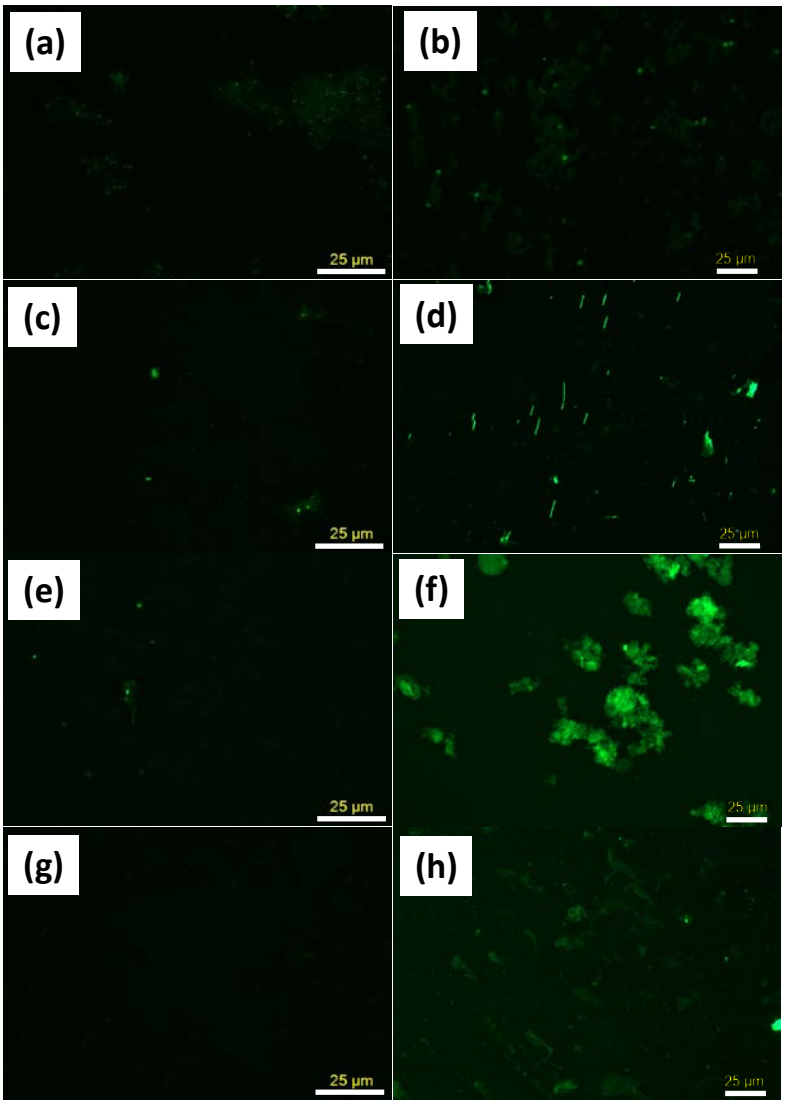

Figure S6. Fluorescence microscopic images of histidine based hydrogels after incubation with ThT. (a, b) Fmoc-HF-COOH in sol and gel state, (c,d) Fmoc-HL-COOH in sol and gel state,(e,f) Fmoc-HV-COOH in sol and gel state, (g,h) Fmoc-HS-COOH in sol and gel state.

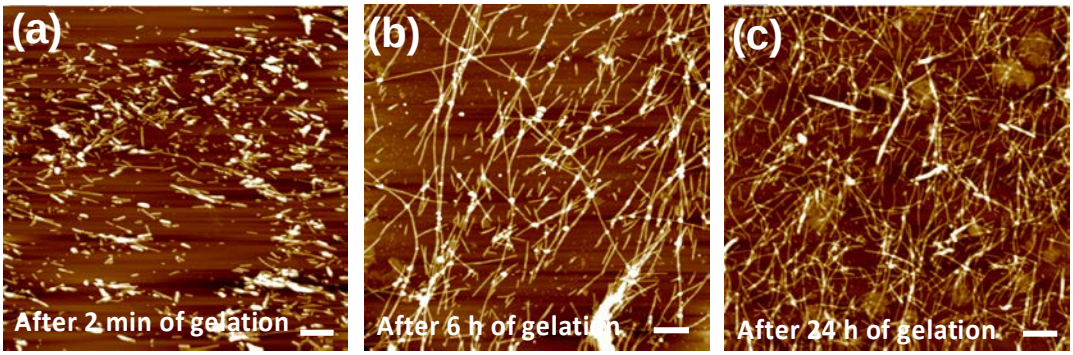

Figure S7. AFM analysis of Fmoc-HL-COOH at different time intervals after gelation showing the growth of the fibers. Scale bar 1μm.

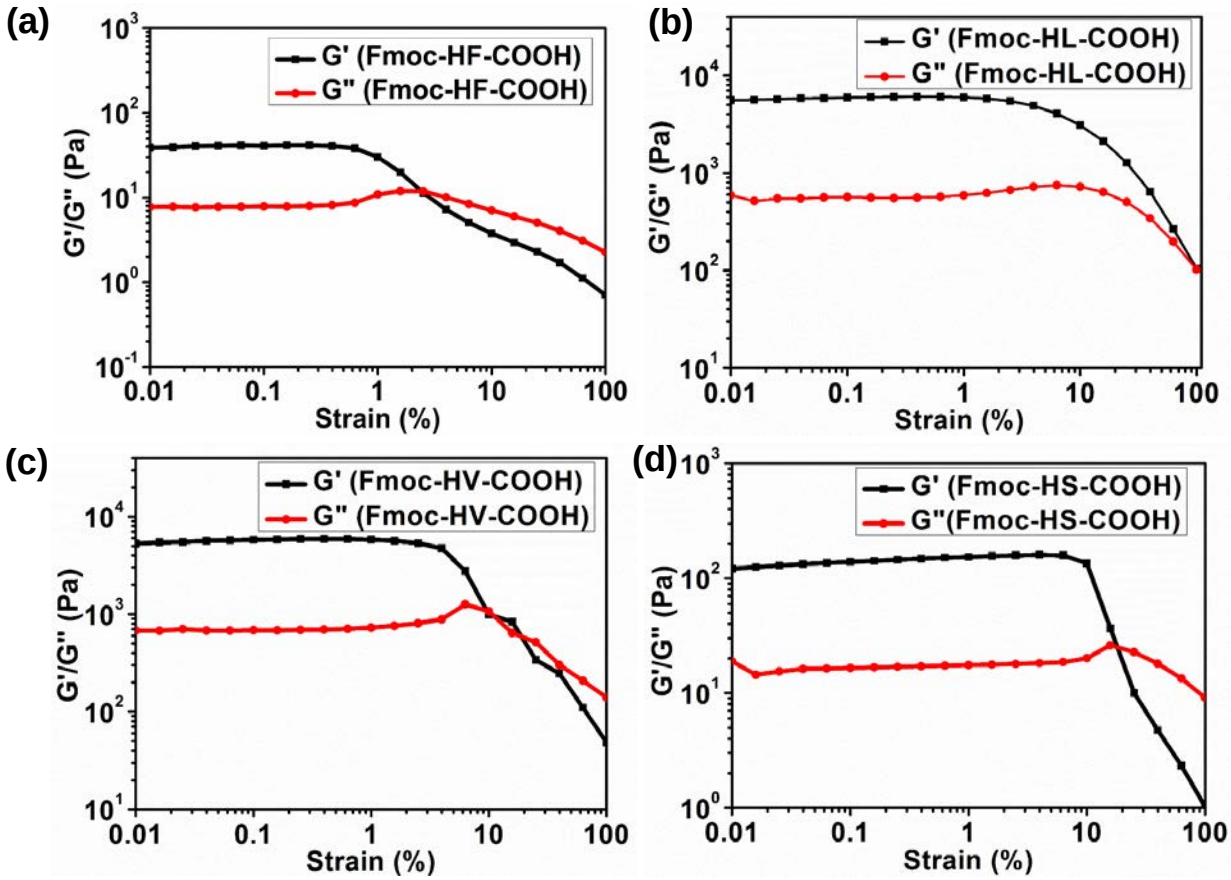

Figure S8. Strain sweep analysis of histidine based hydrogels, (a) Fmoc-HF-COOH, (b) Fmoc-HL-COOH, (c) Fmoc-HV-COOH, (d) Fmoc-HS-COOH.

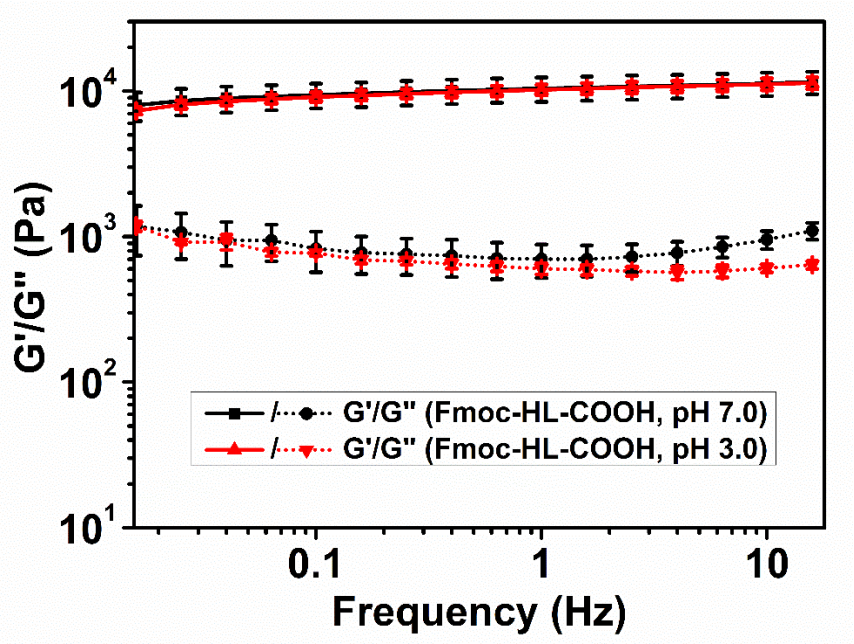

Figure S9. Mechanical strength of Fmoc-HL-COOH hydrogel at variable pH as measured using oscillatory rheology.

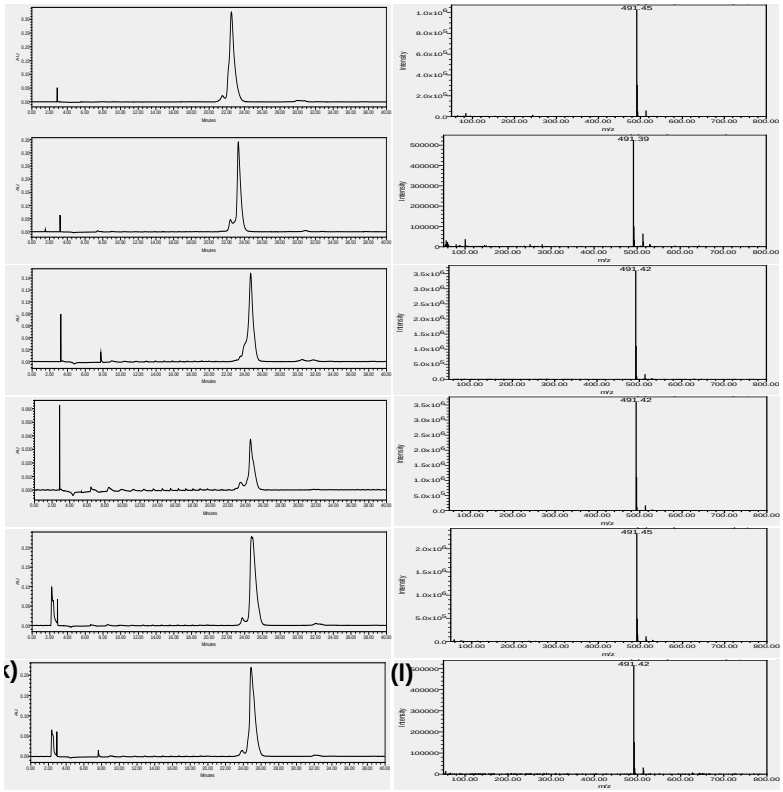

Figure S10. Representative HPLC chromatogram and mass spectra of Fmoc-HL-COOH in the presence of (a,b) iron (II) chloride salt, (e, f) magnesium chloride salt, (i, j) copper (II) chloride salt, immediately after adjusting the pH to 10.0, and in the presence of (c, d) iron (II) chloride salt, (g,h) magnesium chloride salt, (k,l) copper (II) chloride salt after pH was adjusted to 7.0 respectively. Both the analysis confirmed that the pH switch used to dissolve the peptides in the presence of salts did not cleave the fluorenyl moiety from the peptide.

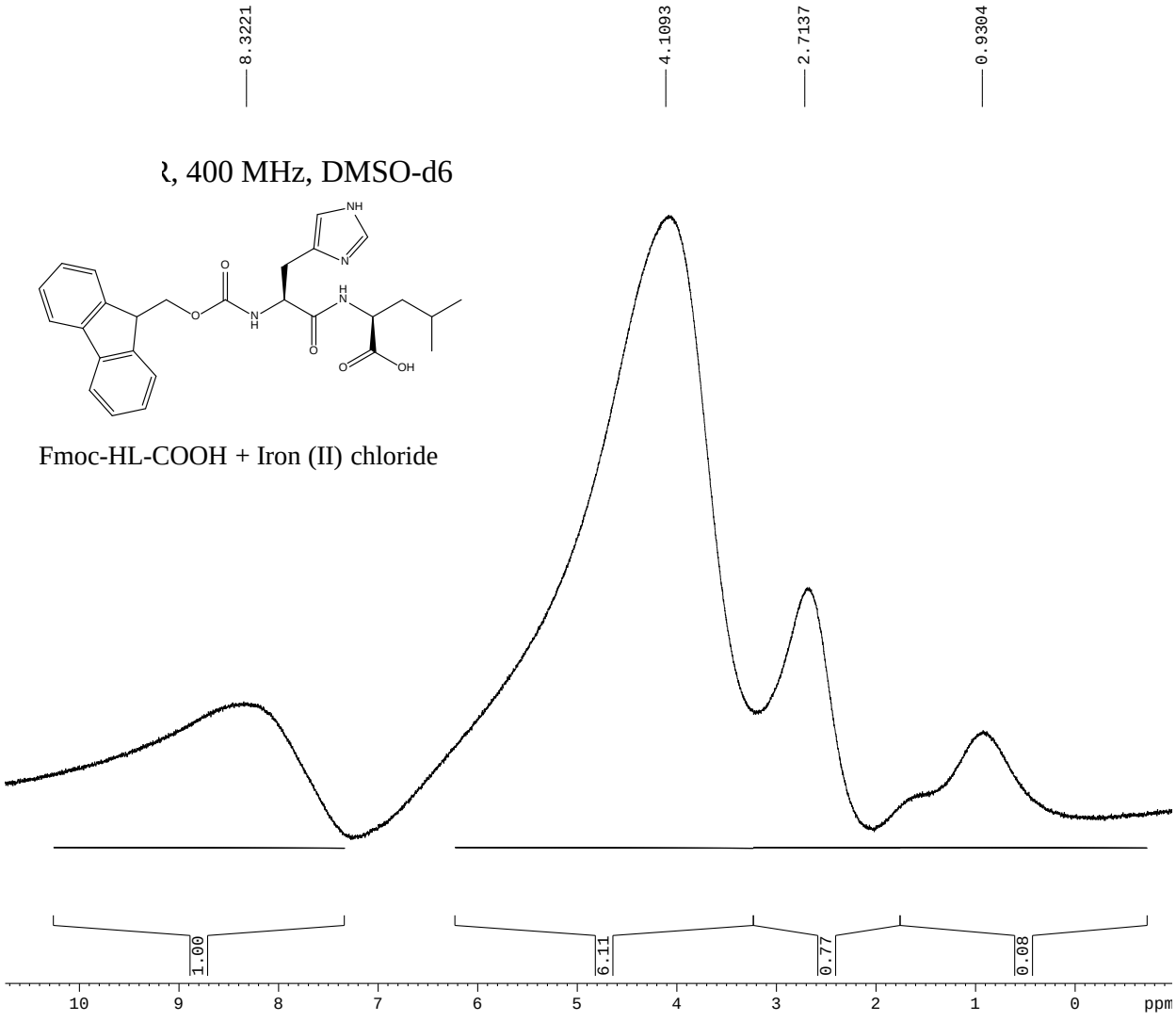

Figure S11. ^{1}H-NMR spectrum of lyophilized hydrogel of Fmoc-HL-COOH formed in the presence of iron (II) chloride, showing significant NMR peak broadening.

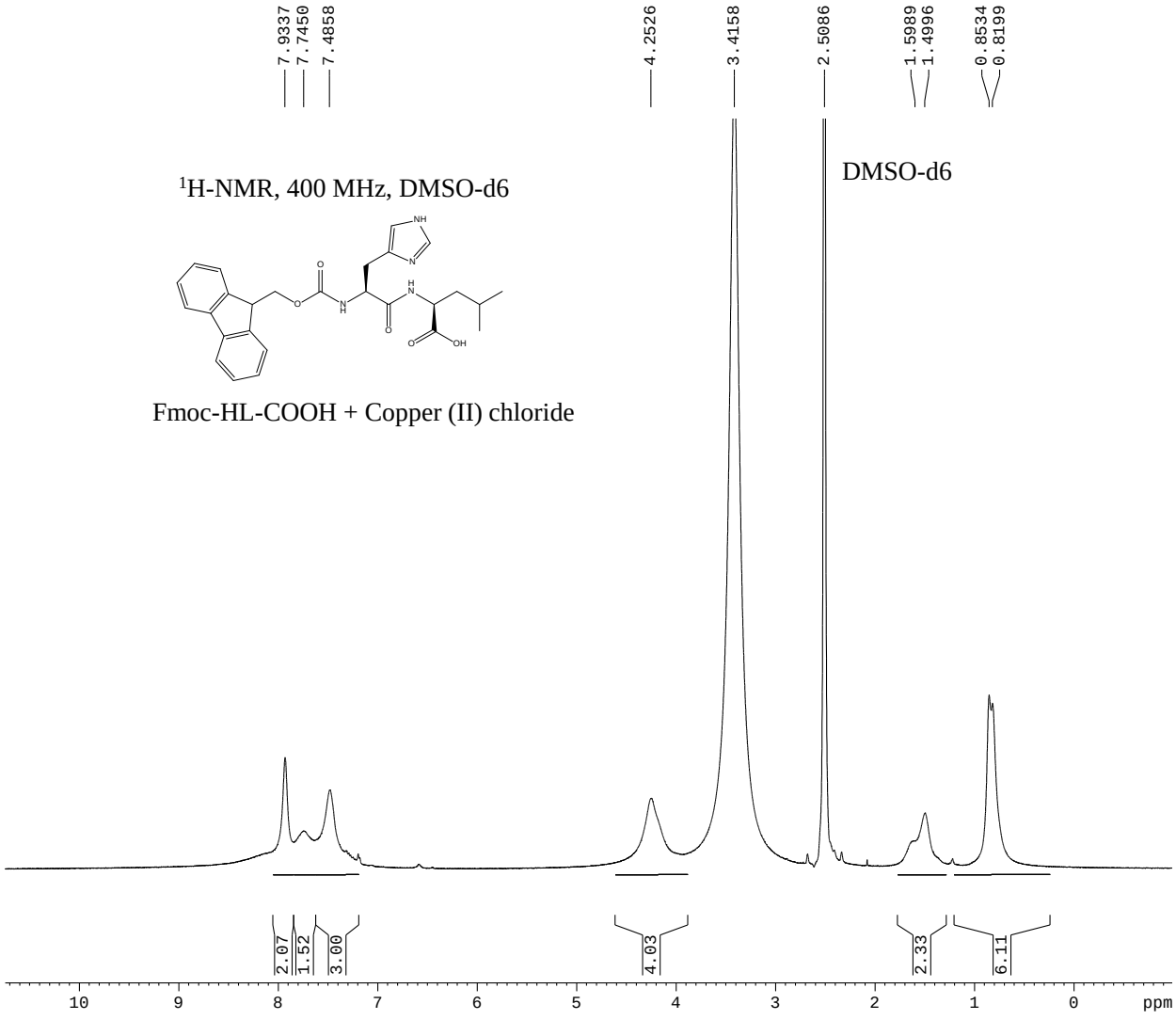

Figure S12. ^{1}H-NMR spectrum of lyophilized hydrogel of Fmoc-HL-COOH formed in the presence of copper (II) chloride, showing significant NMR peak broadening.

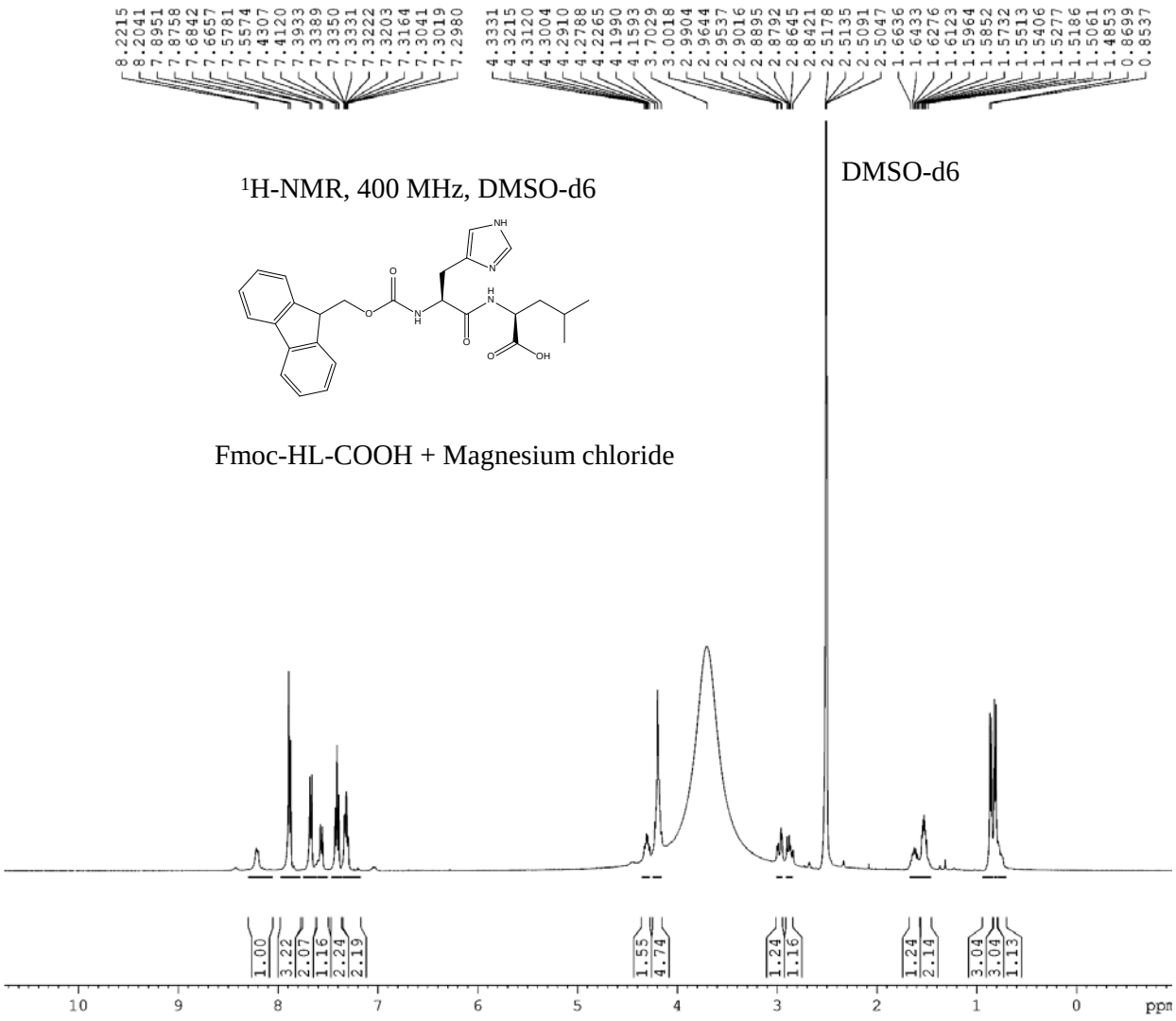

Figure S13. ^{1}H-NMR spectrum of lyophilized hydrogel of Fmoc-HL-COOH formed in the presence of magnesium chloride, demonstrating the integrity of the fmoc group during gelation.

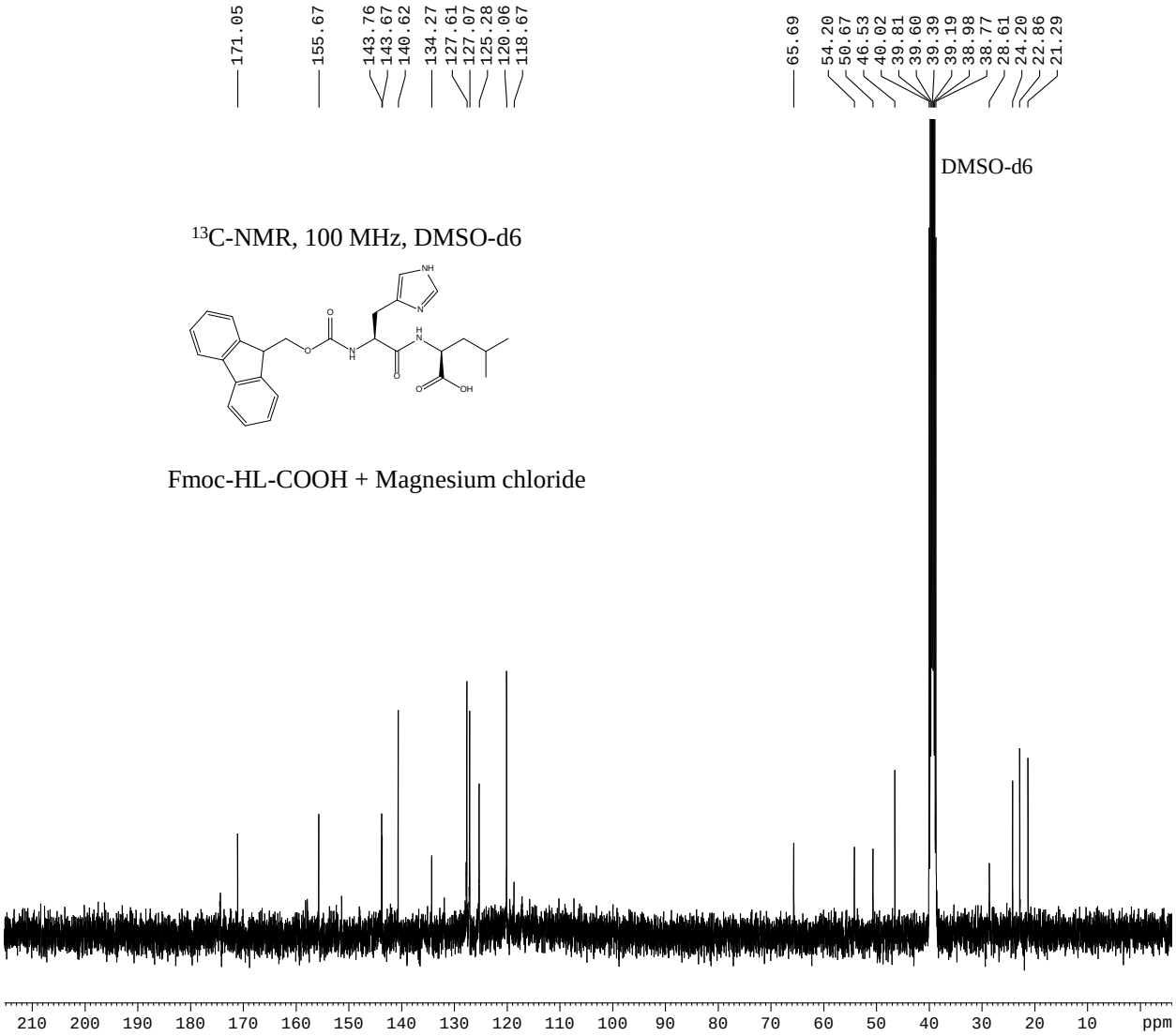

Figure S14. ^{13}C-NMR spectrum of lyophilized hydrogel of Fmoc-HL-COOH formed in the presence of magnesium chloride, demonstrating the integrity of the fmoc group during gelation.

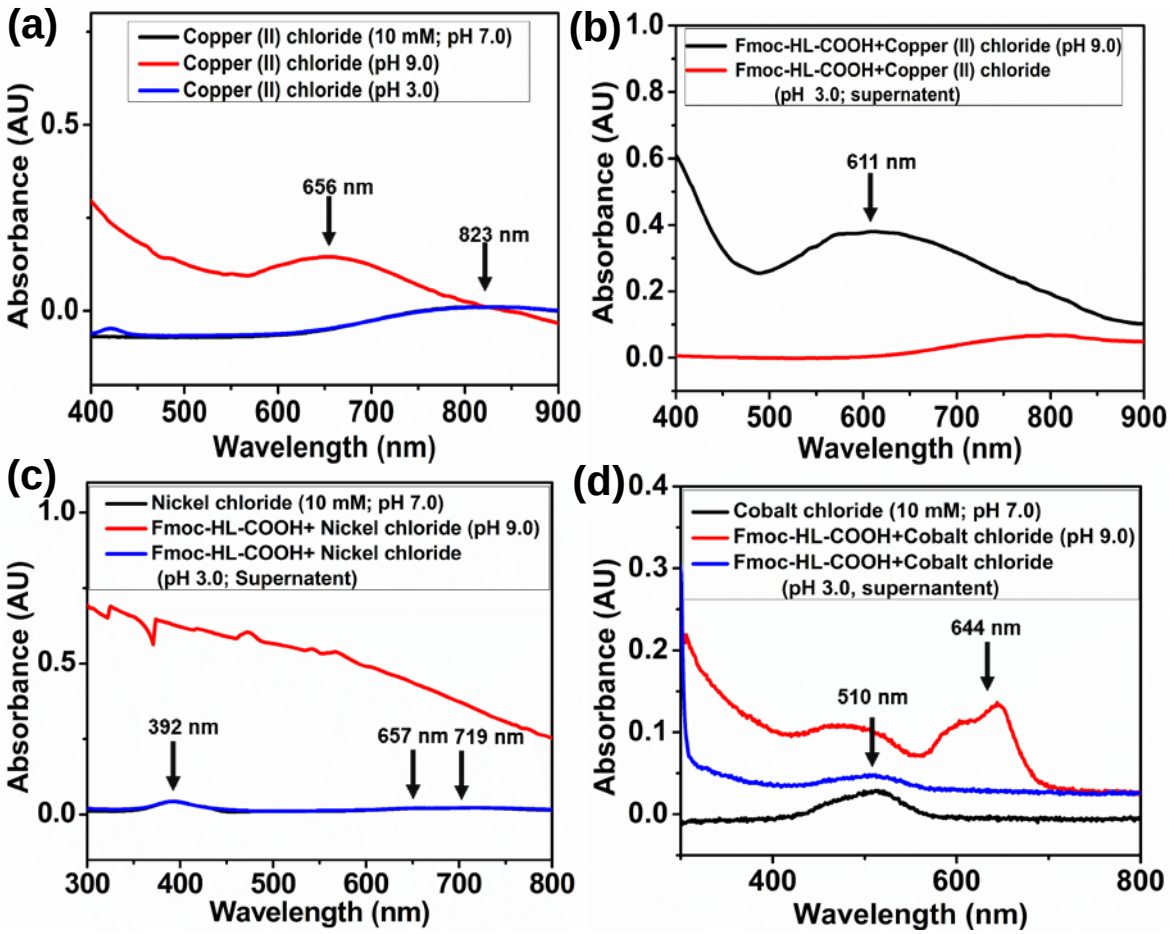

Figure S15. UV-Vis spectra of (a) copper (II) chloride (10 mM)at both acidic and basic pH, (b) copper (II) chloride (10 mM), in the presence of Fmoc-HL-COOH (20 mM) showing the formation of peptide copper complex in basic pH. UV-Vis spectra of (c) nickel chloride and (d) cobalt chloride at acidic and basic pH in the presence of Fmoc-HL-COOH, showing the formation of peptide-metal complex at pH 9.0.

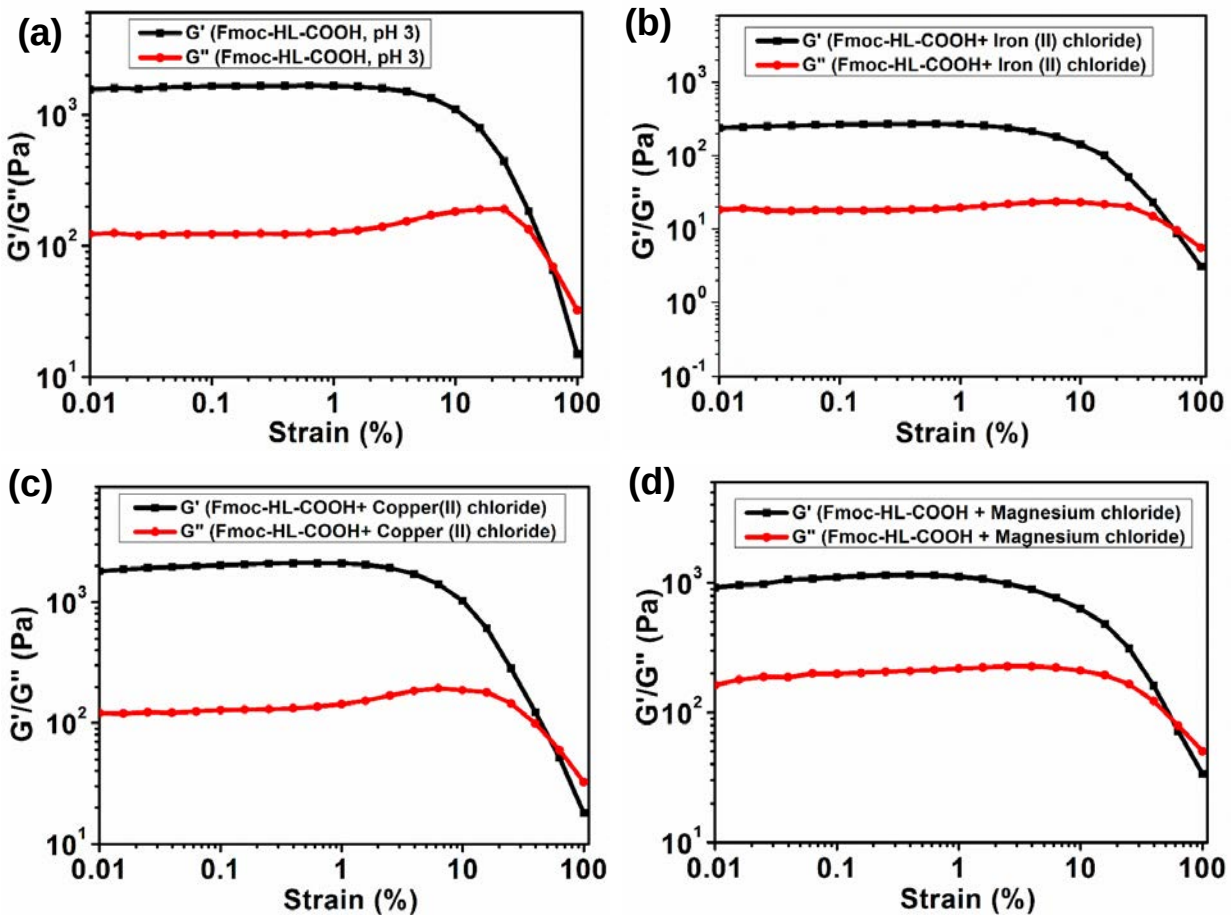

Figure S16. Strain sweep analysis of (a) Fmoc-HL-COOH at 10 mM, Fmoc-HL-COOH (10 mM) in the presence of (b) iron (II) chloride (10 mM), (c) copper (II) chloride (10 mM), (d) magnesium chloride (10 mM).

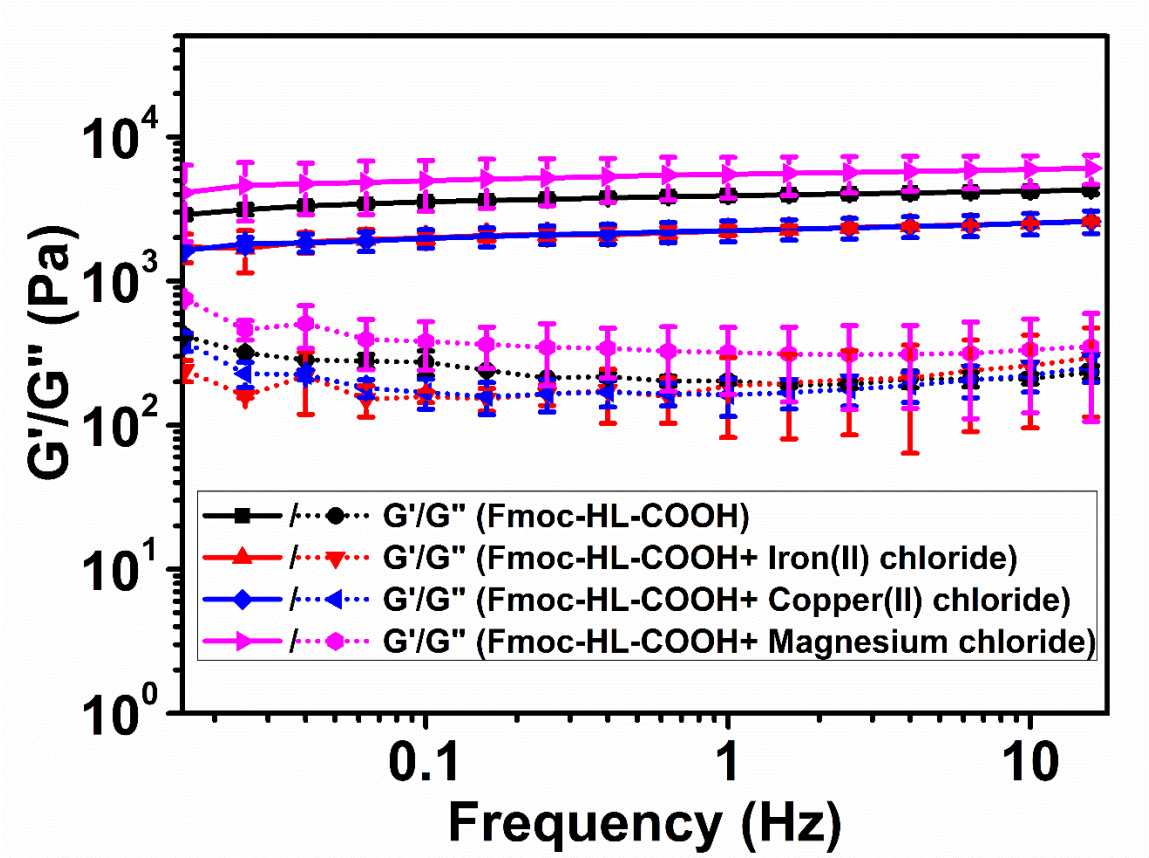

Figure S17. Mechanical strength of Fmoc-HL-COOH (10 mM) in the presence of salts at a concentration of 10 mM each.

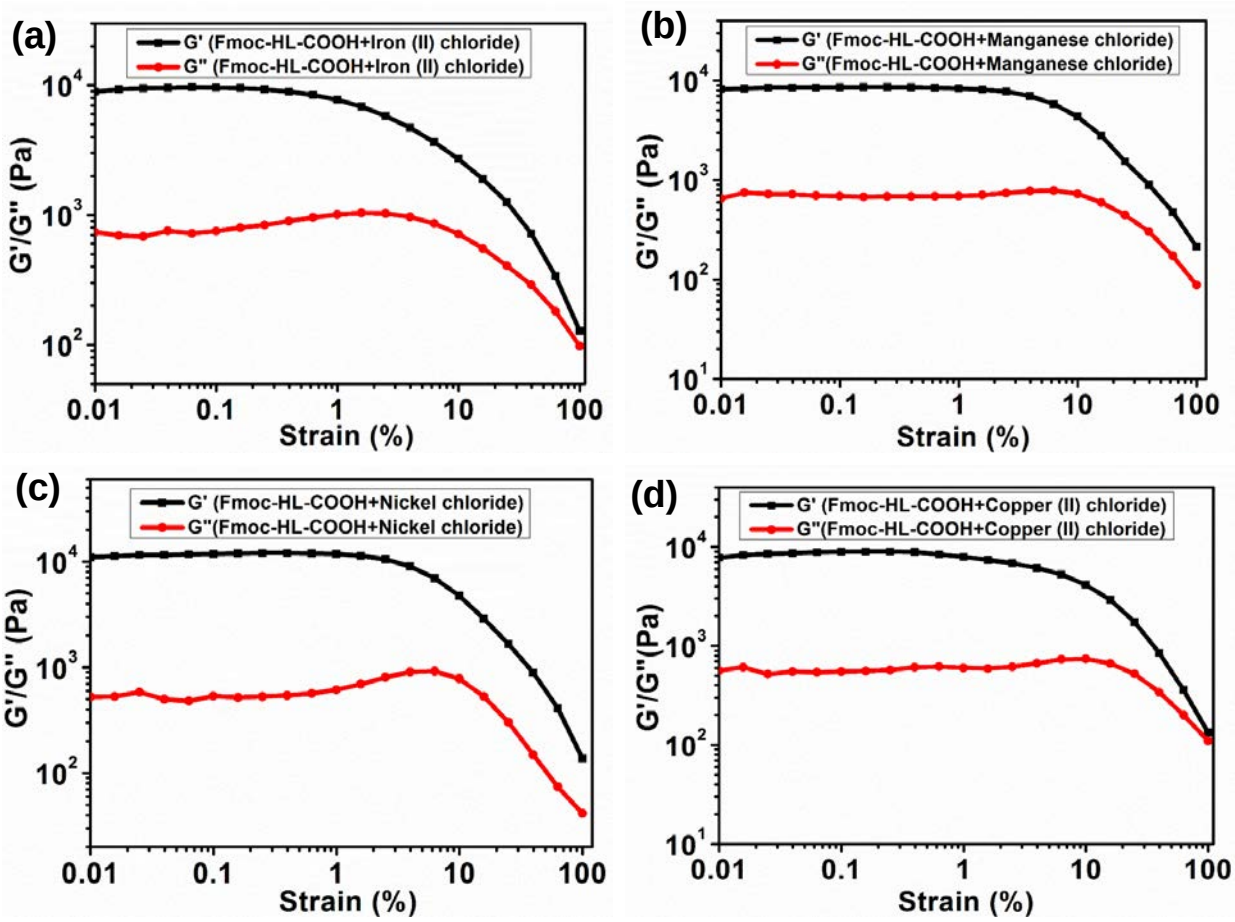

Figure S18. Strain sweep analysis of Fmoc-HL-COOH (20 mM) in the presence of (a) iron (II) chloride, (b) manganese chloride, (c) nickel chloride, (d) copper (II) chloride.

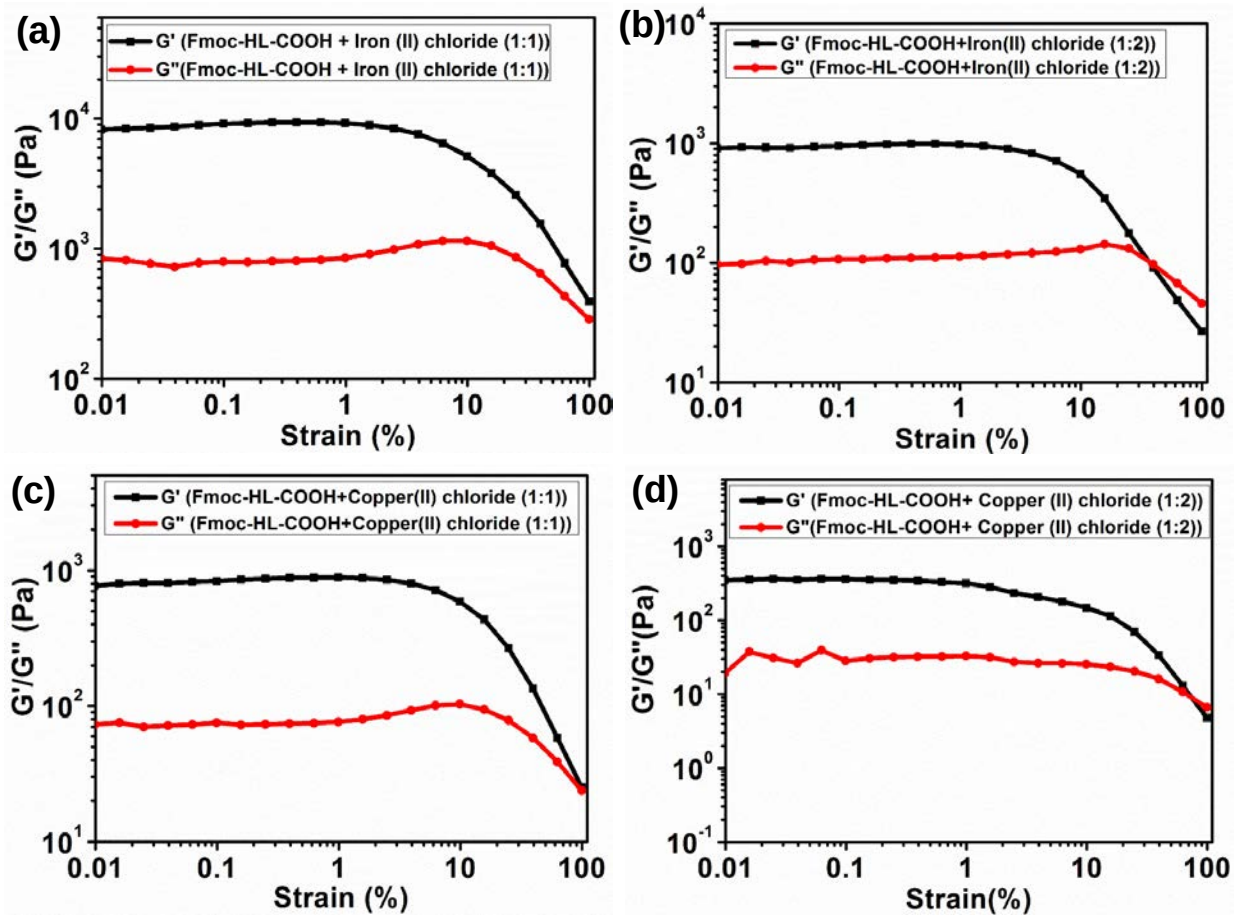

Figure S19. Strain sweep analysis of Fmoc-HL-COOH in the presence of (a) iron (II) chloride (1:1), (b) iron (II) chloride (1:2), (c) copper (II) chloride (1:1), (d) copper (II) chloride (1:2).

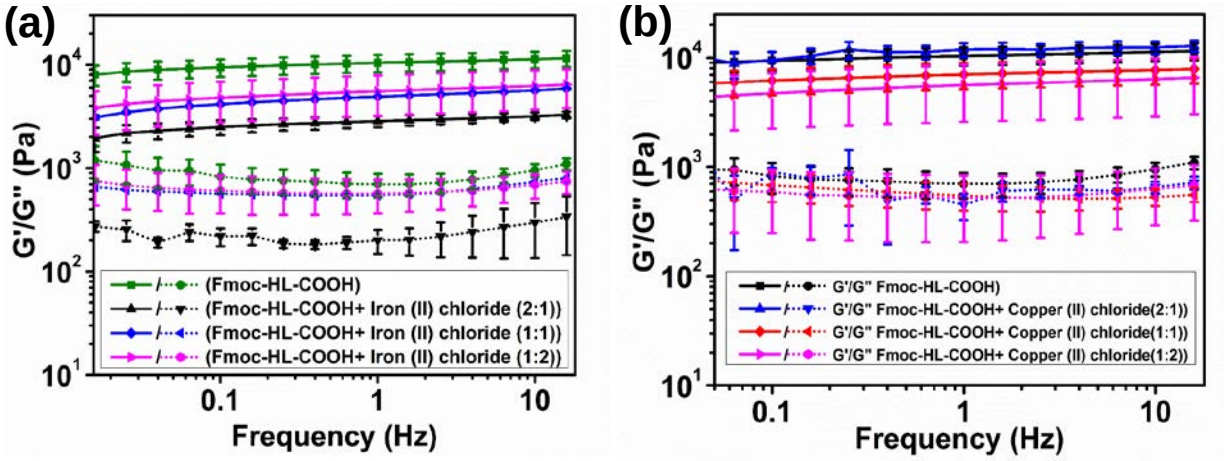

Figure S20. Variation in mechanical strength of Fmoc-HL-COOH with varying ratio of (a) iron (II) chloride and (b) copper (II) chloride as measured by oscillatory rheology.

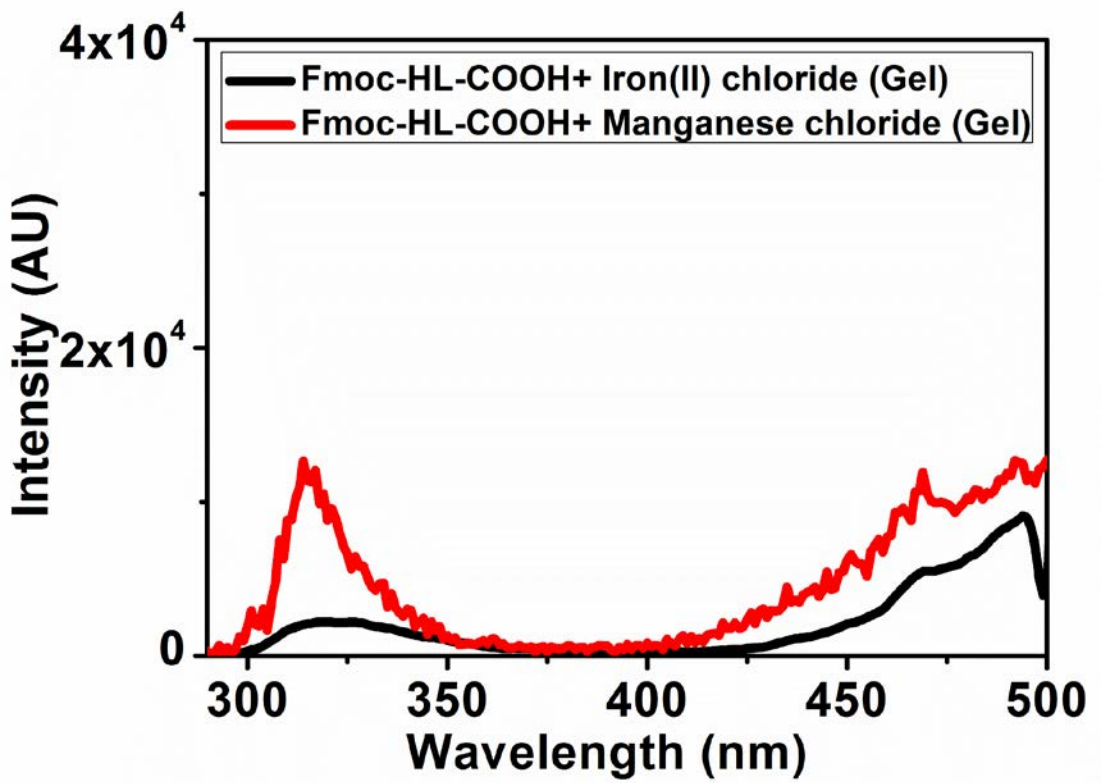

Figure S21. Magnified view of figure 7e showing the fluorescence spectra of Fmoc-HL-COOH in the presence of iron (II) chloride and manganese chloride depicting the quenching of fmoc fluorescence upon gelation.

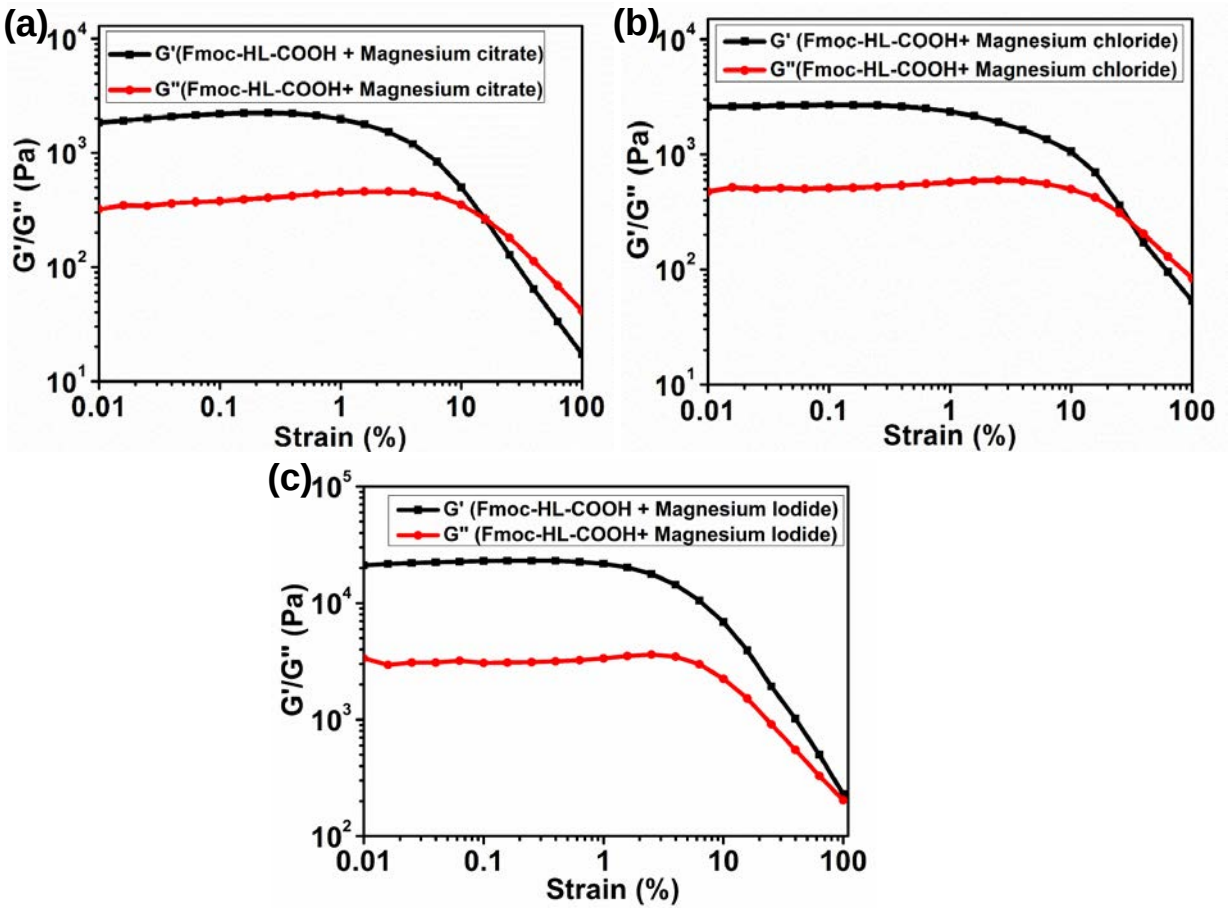

Figure S22. Strain sweep analysis of Fmoc-HL-COOH hydrogel formed in the presence of (a) magnesium citrate, (b) magnesium chloride, (c) magnesium iodide.

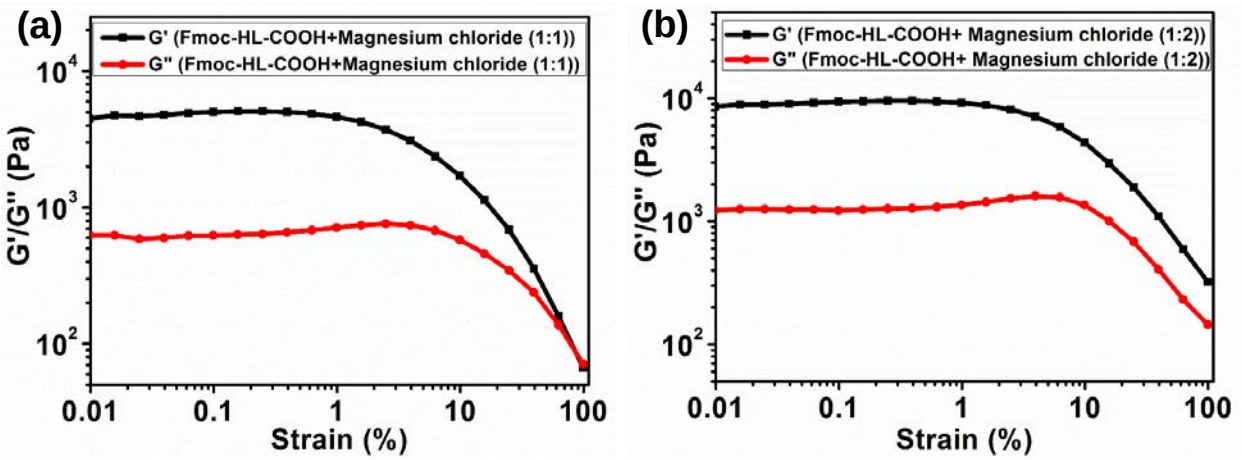

Figure S23. Strain sweep analysis of Fmoc-HL-COOH hydrogel formed in the presence of (a) magnesium chloride (1:1), (b) magnesium chloride (1:2).

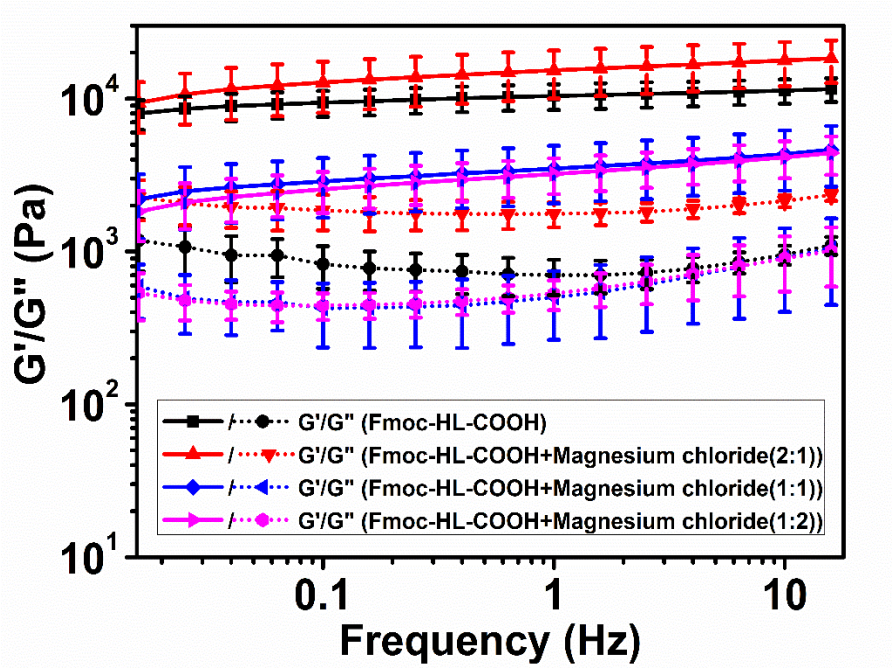

Figure S24. Variation in mechanical strength of Fmoc-HL-COOH with varying ratio of magnesium chloride as measured by oscillatory rheology.

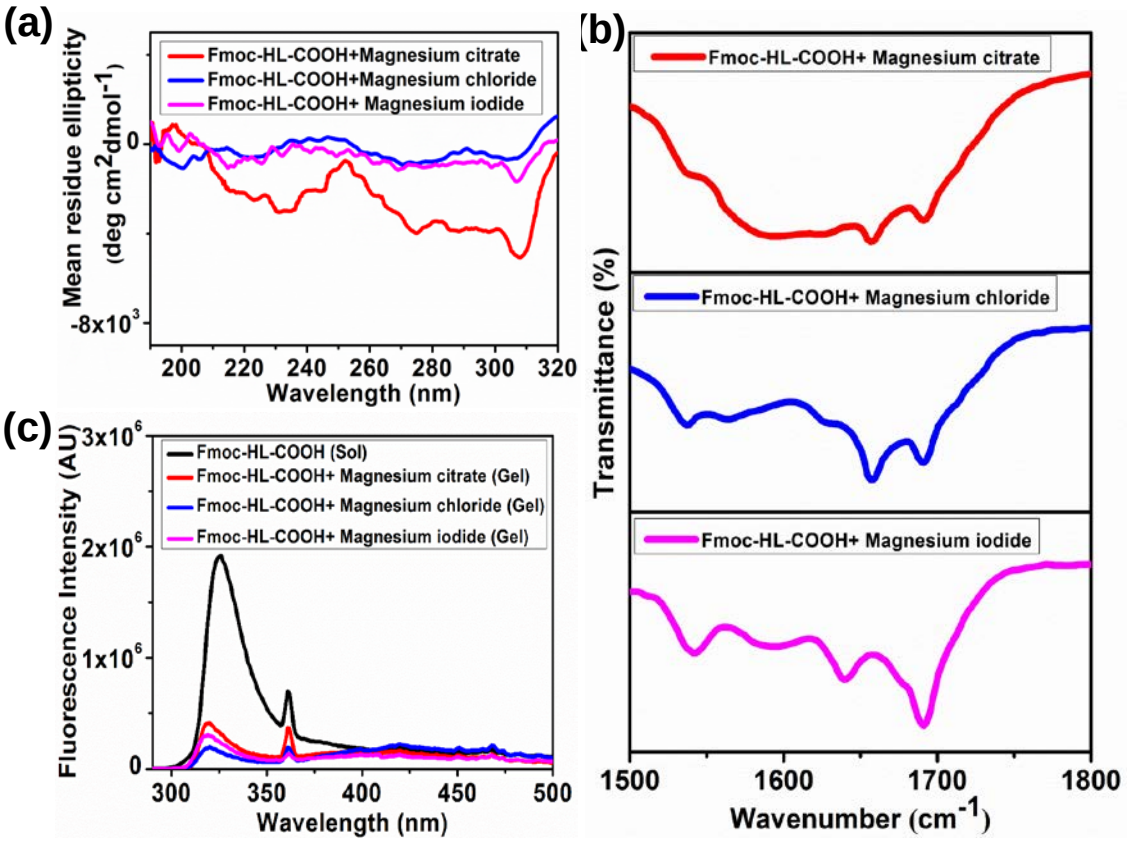

Figure S25. (a) CD spectra showing the change in supramolecular chirality peak of fluorenyl groups in metallogels of Fmoc-HL-COOH with different counter anions of magnesium, (b) FTIR analysis suggesting the presence ofβ-sheet structure in the gel state, (c) Fluorescence spectra of metallogels showing differential extent of quenching of fluorenyl emission upon gelation in the presence of different counter anions of magnesium.

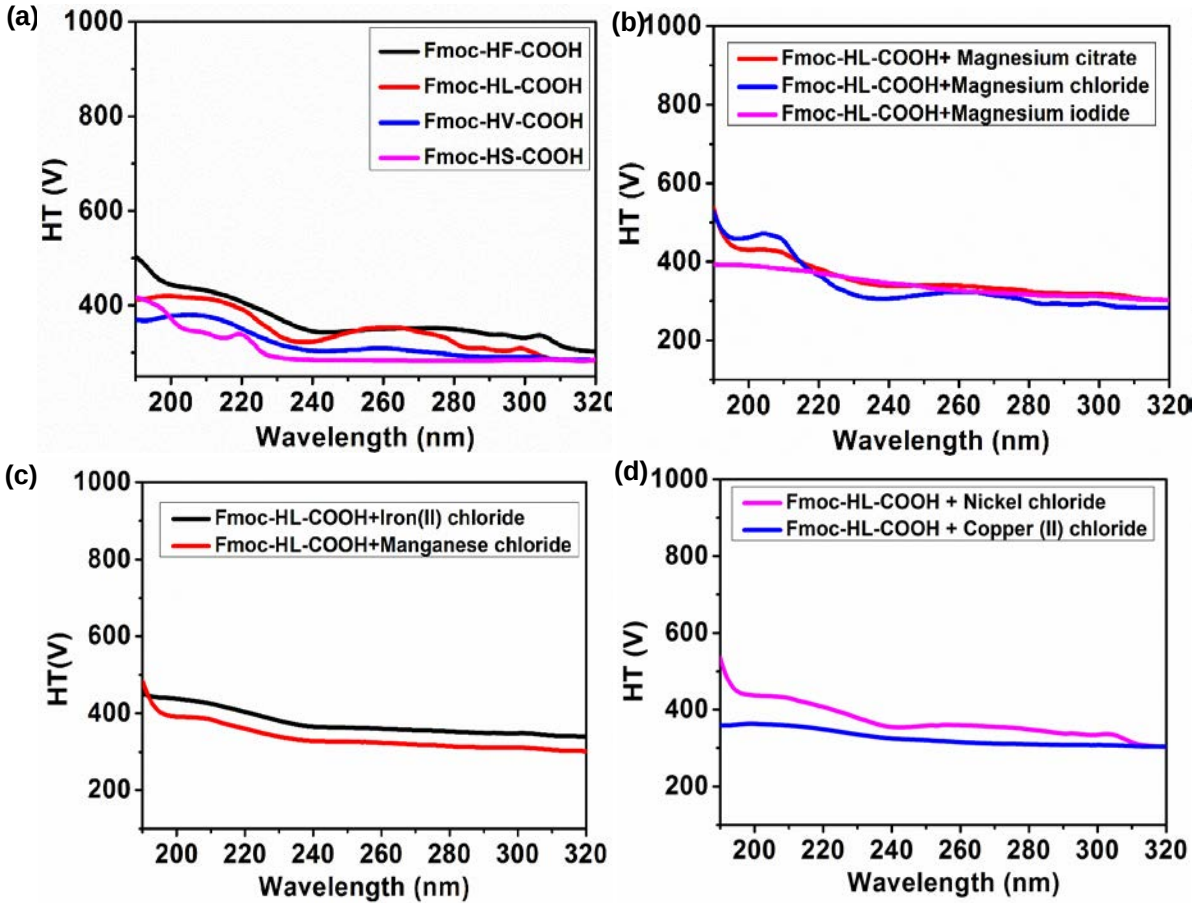

Figure S26. Spectra showing the variation in HT voltage with wavelength in CD spectroscopy for (a) Fmoc conjugated histidine dipeptides, Fmoc-HL-COOH in the presence of (b) magnesium salts, (c) iron and manganese salt, (d) nickel and copper salt respectively.